(a) Verify that at these points, $E = E_F = 0$.

(b) At the six corners of the first Brillouin zone, $|\mathbf{k}| = 4\pi/3a$. Make a two-dimensional plot of the E–k relationship for k_x, k_y extending a bit past $|\mathbf{k}|$. Verify that the bonding and antibonding bands touch at the six points of the first Brillouin zone hexagon, showing that graphene is a semimetal (sometimes called a zero bandgap semiconductor). Also make a one-dimensional plot of $E\left(0, k_y\right)$ for $-|\mathbf{k}| \leq k_y \leq |\mathbf{k}|$, showing that the bands touch at $E = 0$ at $k_y = \pm 4\pi/3a$.

22. What is the radius of a $(19, 0)$ carbon nanotube? Repeat for a $(10, 10)$ nanotube. Consider an $(n, 0)$ zigzag carbon nanotube that has radius 0.3523 nm. What is the value of the index n?

23. Since carbon nanotubes are only periodic along their axis, the transverse wavenumber becomes quantized by the finite circumference of the tube. Derive (5.66) and (5.67) by enforcing the condition that an integer number q of transverse wavelengths must fit around the tube ($k_\perp = 2\pi/\lambda_\perp$).

24. Using (5.68) and (5.69), plot the dispersion curves for the first eight bonding and antibonding bands in a $(5, 5)$, $(9, 0)$, and $(10, 0)$ carbon nanotube. Let the axial wavenumber vary from $k = 0$ to $k = \pi/a_{ac}$ for the armchair tube, and from $k = 0$ to $k = \pi/a_{zz}$ for the zigzag tube. Comment on whether each tube is metallic or semiconducting, and identify the band (i.e., the q value) that is most important. If the tube is semiconducting, determine the approximate band gap.

Part II

SINGLE-ELECTRON AND FEW-ELECTRON PHENOMENA AND DEVICES

In previous chapters, Schrödinger's equation and the principles of quantum physics were developed, with an emphasis on single particles (primarily electrons) and collections of noninteracting particles in different spatial regions. The remainder of the text is divided into two parts, and presents some basic nanoelectronic applications of these principles. In the next part, we will be concerned with physical phenomena associated with single electrons, or small numbers of electrons (perhaps, say, 10^0–10^5 electrons). The main emphasis is on electrons confined to nanoscopic spaces, such as quantum dots, and devices constructed from quantum dots and "charge islands." Nanoelectronics principles are developed for the so-called "single-electron" devices, including the single-electron transistor, after the important concept of Coulomb blockade has been discussed. Although most single-electron devices are at an early stage of development, especially in the area of manufacturability, they offer the potential benefits of ultralarge scale integration, with device dimensions on the order of nanometers. They also may exhibit very low power dissipation, and high speed. All of these positive attributes arise from the need to move only single electrons, or small groups of electrons, through devices.

The use of the term "single-electron" device merits some discussion. In conventional microelectronics, currents are typically on the order of 1 μA to 1 mA, corresponding to the movement of 6.25×10^6–6.25×10^9 electrons per microsecond. This occurs through a device perhaps 100 nm in length. Even considering devices at the upper limit of optical

lithography, perhaps on the order of 10^5 electrons are involved in performing, for example, a digital operation. In the following chapters, conversely so-called "single-electron" devices are studied. In fact, this is a bit of a misnomer, and in the literature the term "single-electron precision" device has been suggested as a more descriptive name. This allows for the fact that usually much more than one electron is involved, although the number may be relatively small, perhaps 10–10, 000 electrons. It is important to note that these devices are typically sensitive to the transfer of a single electronic charge, and therefore they can operate by manipulating an extremely small number of electrons. However, this generally positive attribute has it "dark side" as well. For example, if a device is sensitive to the movement of a single electronic charge, then the presence of a single charge impurity, in, say, an oxide layer, may drastically influence device operation.

Chapter

6

TUNNEL JUNCTIONS AND APPLICATIONS OF TUNNELING

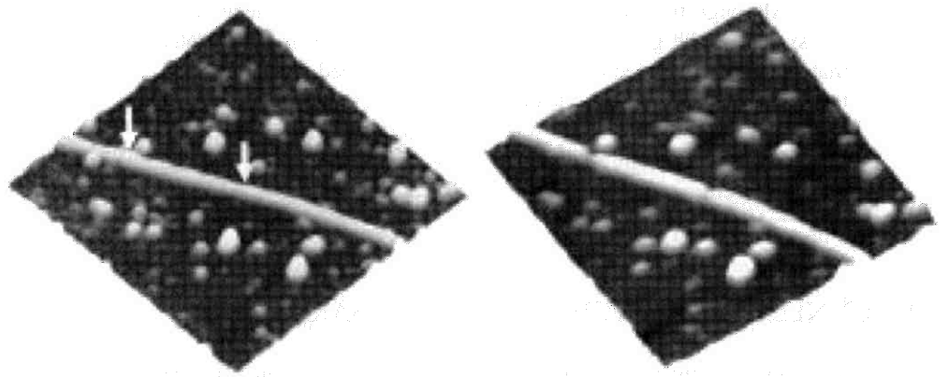

(a) (b)

Quantum dot formed by cutting a carbon nanotube. Transport through the dot is via tunneling. Image size is 500 × 500 nm^2, and the height of the tube is 3 nm. (From Park, J.-Y., et al., "Electrical Cutting and Nicking of Carbon Nanotubes Using an Atomic Force Microscope." *Appl. Phys. Lett.*, 80 (2002): 4446. © 2002, American Institute of Physics.)

In Chapter 4, the general concept of a quantum dot was introduced. A very important aspect to consider is the connection of the quantum dot to the "outside world," or, alternatively, the interaction of a quantum dot with the outside world. In the second case, we often want to "interrogate" the dot remotely. For example, we may want the dot to glow (i.e., emit photons) when illuminated with radiation, in order to be used as a marker, for, say, locating a cancer cell to which the dot is attached. We may even want the dot to cause sufficient heating of the cell to kill it, which has, in fact, already been used in the treatment of skin cancer. This type of application will be further described in Chapter 9.

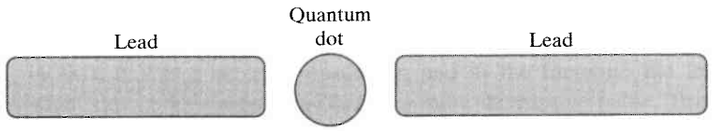

Figure 6.1 Nano-object coupled to external leads.

In this chapter and the next, we want to consider the first scenario, where we "connect" a quantum dot to wires via tunnel junctions, in order to form an electronic device such as a transistor. Not only is this a practical issue, but also, as it turns out, it is one that leads to interesting phenomena and useful applications. In particular, we want to study a method of "communicating" with a nanoscopic object by bringing electrical leads into close proximity to, but not making contact with, the object. This is depicted schematically in Fig. 6.1, which shows a quantum dot separated from two leads by an insulating region.

Although the leads do not contact the object, d.c. electrical current can pass through the system if the gap between the leads and the dot is sufficiently small, despite the fact that the gap is modeled as a perfect insulator. Indeed, the connection between the object and the outside world (i.e., the leads) is by a process known as *quantum tunneling*, or simply tunneling, and in this chapter we consider tunneling in a general sense. In the next chapter, the concept of tunneling is applied to the interaction of the dot and electrical leads, and to related structures such as the single electron transistor.

6.1 TUNNELING THROUGH A POTENTIAL BARRIER

The topic of tunneling is very important for nanoelectronic devices, and is used fruitfully in a large number of applications. We will consider some of these in the next few sections; however, we first consider a general tunneling problem.

To investigate tunneling, consider a particle such as an electron, incident from the left on a potential energy barrier, as depicted in Fig. 6.2.

The potential energy profile is given by

$$V = \begin{cases} V_0, & 0 \le x \le a, \\ 0, & x < 0,\ x > a, \end{cases} \tag{6.1}$$

which models, for example, the energy profile in a metal–insulator–metal junction, as discussed subsequently. Other, qualitatively similar potential energy profiles model an electron bound to an atom or molecule, an electron bound to a quantum dot, and similar confinement structures. We make the assumption that the barrier does not contain any scattering objects, so that particles transverse the barrier coherently.† This assumption allows one to

†Certain collisions between particles would lead to incoherent transport, as further discussed in Chapter 10.

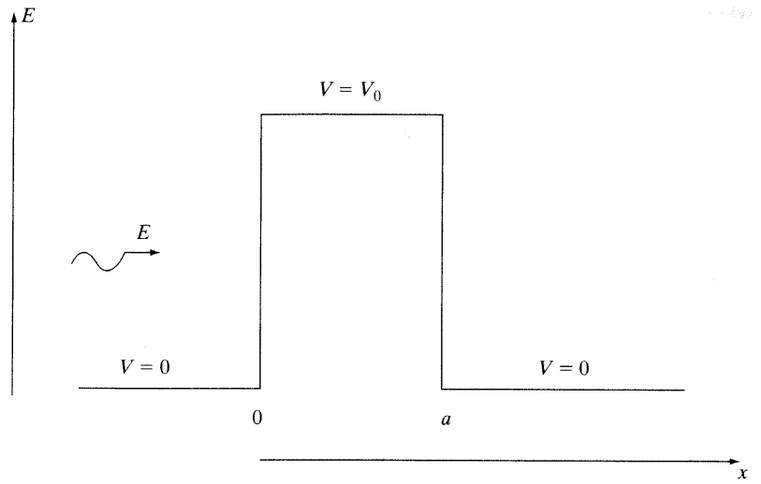

Figure 6.2 Particle with energy E incident on a potential barrier.

solve Schrödinger's equation with boundary/continuity conditions applied at the barrier's interfaces, rather than at various points inside the barrier.

We are interested in two cases; when the particle has total energy $E > V_0$, and when $E < V_0$. According to classical physics, for $E > V_0$, the particle will simply move past the potential barrier. This would happen with 100 percent certainty. (Its transmission coefficient would be unity, and its reflection coefficient would be zero.) For the case $E < V_0$, the particle would be reflected from the barrier with 100 percent certainty. (Its transmission coefficient would be zero, and its reflection coefficient would be unity.) However, quantum mechanics shows a more complicated behavior.

Starting with Schrödinger's equation,

$$\left(-\frac{\hbar^2}{2m^*}\frac{d^2}{dx^2} + V(x)\right)\psi(x) = E\psi(x), \tag{6.2}$$

we note that it is difficult to solve (6.2) when $V(x)$ varies as a function of position (i.e., in this case, Schrödinger's equation is a nonconstant coefficient differential equation). If $V(x)$ is a piecewise constant function, the usual method to avert this problem is to solve Schrödinger's equation separately in each region where V is constant, and to connect the solutions using the boundary conditions for the wavefunction, (3.143).

Proceeding in this manner, in region I ($x < 0$) where $V = 0$, we find that Schrödinger's equation is

$$-\frac{\hbar^2}{2m^*}\frac{d^2}{dx^2}\psi_1(x) = E\psi_1(x), \tag{6.3}$$

which has solutions

$$\psi_1(x) = Ae^{ik_1x} + Be^{-ik_1x}, \tag{6.4}$$

where

$$k_1^2 = \frac{2m^* E}{\hbar^2}. \tag{6.5}$$

In region II ($0 \leq x \leq a$) where $V = V_0$, Schrödinger's equation is

$$\left(-\frac{\hbar^2}{2m^*}\frac{d^2}{dx^2} + V_0\right)\psi_2(x) = E\psi_2(x), \tag{6.6}$$

which has solutions

$$\psi_2(x) = Ce^{ik_2x} + De^{-ik_2x}, \tag{6.7}$$

where

$$k_2^2 = \frac{2m^*(E - V_0)}{\hbar^2}. \tag{6.8}$$

Note that for the case $E \lesseqgtr V_0$,

$$k_2^2 = \frac{2m^*(E - V_0)}{\hbar^2} \lesseqgtr 0, \tag{6.9}$$

and so k_2 is either pure imaginary or real valued.

Lastly, in region III ($x > a$), Schrödinger's equation is

$$-\frac{\hbar^2}{2m^*}\frac{d^2}{dx^2}\psi_3(x) = E\psi_3(x), \tag{6.10}$$

which has solutions

$$\psi_3(x) = Fe^{ik_3x} + Ge^{-ik_3x}, \tag{6.11}$$

where

$$k_3^2 = \frac{2m^*E}{\hbar^2} = k_1^2. \tag{6.12}$$

Since there is no potential disturbance to reflect the wave after it reaches region III, $G = 0$.

Therefore, we have

$$\begin{aligned}\psi_1(x) &= Ae^{ik_1x} + Be^{-ik_1x}, \\ \psi_2(x) &= Ce^{ik_2x} + De^{-ik_2x}, \\ \psi_3(x) &= Fe^{ik_1x}.\end{aligned} \tag{6.13}$$

Note that since in region III $|\psi_3|^2$ is constant, the particle is equally likely to be found at any point in this region.

The boundary conditions (3.143), and continuity of ψ and ψ' at $x = 0$ and at $x = a$, lead to

$$\begin{aligned}\frac{B}{A} &= \frac{\left(k_1^2 - k_2^2\right)\left(1 - e^{i2ak_2}\right)}{(k_1 + k_2)^2 - (k_1 - k_2)^2 e^{i2ak_2}}, \\ \frac{F}{A} &= \frac{4k_1k_2e^{i(k_2 - k_1)a}}{(k_1 + k_2)^2 - (k_1 - k_2)^2 e^{i2ak_2}}.\end{aligned} \tag{6.14}$$

We can define a *tunneling probability* as

$$T = \left|\frac{F}{A}\right|^2 = \frac{4E(E - V_0)}{V_0^2 \sin^2(k_2a) + 4E(E - V_0)}, \tag{6.15}$$

which is obviously the modulus squared of the ratio of the transmitted to incident wavefunctions. We can define a *reflection probability* as

$$R = \left|\frac{B}{A}\right|^2 = \frac{V_0^2 \sin^2(k_2a)}{V_0^2 \sin^2(k_2a) + 4E(E - V_0)}, \tag{6.16}$$

which is the modulus squared of the ratio of the reflected to incident wavefunctions.

If $E < V_0$, then, classically, the particle would be turned back by the barrier ($T = 0$, $R = 1$), whereas, classically, for $E > V_0$ the particle would move unimpeded past the barrier ($T = 1$, $R = 0$). However, consider the plot of $T(E)$ versus E, as shown in Fig. 6.3. It can be seen that the classical values are limiting cases for $E \ll V_0$ and $E \gg V_0$. In general, however, for most values of energy $0 < T < 1$, meaning that there is some nonzero probability that the electron will be transmitted through the barrier. For larger values of

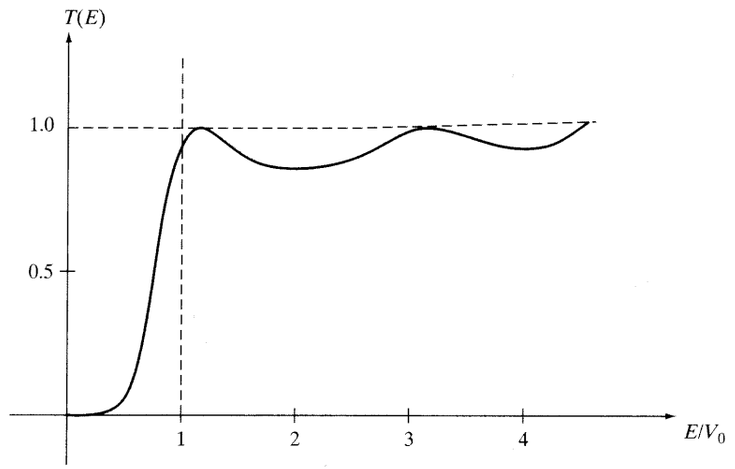

Figure 6.3 Tunneling probability versus energy for a potential energy barrier.

energy, it is more likely that the electron will be transmitted through the barrier, but even for relatively large energies the electron may be reflected by the barrier.

If the electron is transmitted through the barrier in the case $E < V_0$, the electron is said to *tunnel through the barrier* for the following reason. The total energy of the electron is the sum of kinetic and potential energies,

$$E = E_{KE} + E_{PE} \tag{6.17}$$

$$= E_{KE} + V_0, \quad \text{inside the barrier,} \tag{6.18}$$

$$= E_{KE} + 0, \quad \text{outside the barrier.} \tag{6.19}$$

If $E < V_0$, then inside the barrier,

$$E = E_{KE} + V_0 < V_0, \tag{6.20}$$

which indicates that the electron's kinetic energy would be negative (i.e., $(1/2)mv^2 < 0$), as discussed for a similar situation in Section 4.5.1. According to classical physics, kinetic energy cannot be negative, and therefore, classically, for $E < V_0$ the electron cannot be found inside the barrier. Thus, classically, the electron cannot get to the other side of the barrier. However, it is well known from experiments that the electron can indeed cross the barrier, with probability (6.15), and so the electron is said to *tunnel through the barrier* in order to get to the other side. For students familiar with electromagnetics and optics, it can be appreciated that particle tunneling is analogous to evanescent wave propagation (as occurs in total internal reflection, sections of below cutoff waveguides, etc.), although that topic will not be addressed here.

It can be seen that for $E/V_0 > 1$, there is a series of transmission resonances where $T = 1$. Rewriting (6.15) as

$$T = \left(1 + \frac{V_0^2}{4E(E - V_0)} \sin^2(k_2 a)\right)^{-1}, \tag{6.21}$$

we can see that full transmission (i.e., $T = 1$) will occur when

$$\sin(k_2 a) = 0, \tag{6.22}$$

that is, when

$$k_2 a = n\pi, \qquad n = 0, 1, 2, \ldots . \tag{6.23}$$

At these points, the internal reflections "bouncing around" in the barrier that lead to left-moving waves exactly cancel, and only the right-moving waves remain. With $k_2 = 2\pi/\lambda_2$, where λ_2 is the wavelength in region II, (6.23) becomes

$$a = n\frac{\lambda_2}{2}, \tag{6.24}$$

so that complete transmission occurs when the barrier thickness is an integral number of half wavelengths. (This situation is called a *transmission resonance*.) The same phenomenon

is encountered in classical electromagnetics and optics, where electromagnetic energy can pass through a half-wavelength dielectric sheet without reflection.

An important, interesting special case is when $E < V_0$, and a is sufficiently large. In this case, we have

$$\sin\left(\sqrt{\frac{2m_e^*(E - V_0)}{\hbar^2}}a\right) = \sin\left(i\sqrt{\frac{2m_e^*(V_0 - E)}{\hbar^2}}a\right) \tag{6.25}$$

$$= i\sinh\left(\sqrt{\frac{2m_e^*(V_0 - E)}{\hbar^2}}a\right)$$

$$\underset{a\to\infty}{\rightarrow} \frac{i}{2}e^{\sqrt{\frac{2m_e^*(V_0-E)}{\hbar^2}}a} = \frac{i}{2}e^{\alpha a},$$

where

$$\alpha = \sqrt{\frac{2m_e^*(V_0 - E)}{\hbar^2}} > 0, \tag{6.26}$$

so that

$$T \rightarrow \frac{16E(V_0 - E)}{V_0^2}e^{-2\alpha a}. \tag{6.27}$$

Therefore, the tunneling probability is exponentially decaying as a function of the barrier width a. So, as might be expected, the tunneling probability is low for thick barriers, and increases as the barrier thickness decreases. Table 6.1 shows the tunneling probability for a $V_0 = 0.2$ eV barrier for two different barrier widths. It can be seen that a doubling of the barrier width significantly changes the tunneling probability (in a nonlinear manner).

For the example of tunneling across the gate oxide in a MOSFET, this explains why, as oxide thickness is decreased, tunneling can become a significant problem, leading to non-negligible gate currents (as discussed in more detail later). Of course, tunneling is often a beneficial phenomenon. Flat panel displays make use of field emission (Section 6.3.1), which is a tunneling phenomenon, and the basis of the scanning tunneling microscope (described on page 202) is tunneling. Last, many nanoelectric devices rely on tunneling for their operation, as described in the next chapter.

TABLE 6.1 TUNNELING PROBABILITY FOR A 0.2 eV BARRIER FOR TWO DIFFERENT BARRIER WIDTHS.

E (eV)	T ($a = 1$ nm)	T ($a = 2$ nm)
0.01	8.86×10^{-3}	1×10^{-4}
0.10	0.145	6.11×10^{-3}
0.20	0.432	0.160

6.2 POTENTIAL ENERGY PROFILES FOR MATERIAL INTERFACES

Although we have considered tunneling through a simple potential energy barrier in a general sense, it is informative to consider the nature of the potential energy profile itself. That is, we should consider what the potential energy profile represents, and whether or not it is a realistic model. It turns out that, for our purposes, the tunneling barrier will often be associated with the junction between two different materials. We consider this topic in the next section.

6.2.1 Metal–Insulator, Metal–Semiconductor, and Metal–Insulator–Metal Junctions

First of all, the rectangular barrier shown in Fig. 6.2 on page 185 is a fairly gross approximation to the actual potential energy profile usually seen in real tunnel junctions. For example, consider the interface between metal and vacuum. If we supply enough energy to the material, electrons can escape from the metal surface.[†] The amount of energy needed to liberate electrons from the metal's surface is the work function, $e\phi$. (See also Section 5.4.) In considering potential energy problems, $e\phi$ can be thought of as merely a material constant. Furthermore, the energy of electrons in the metal, at least the most important electrons, is the Fermi energy, E_F (Section 4.4), which can also be thought of as simply a material constant.[‡] Therefore, the metal–vacuum junction can be modeled as shown in Fig. 6.4, where E_{vac} is the vacuum energy, and the energy difference $E_{\text{vac}} - E_F$ is, by definition, the work

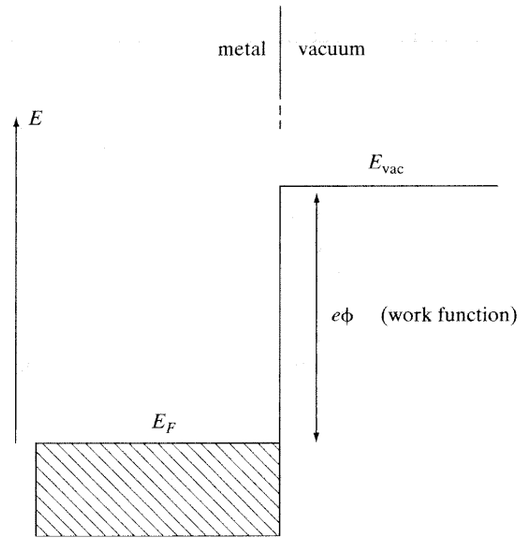

Figure 6.4 Energy band depiction of a metal–vacuum interface.

[†]This is called *thermionic emission* if we supply thermal energy, *photo emission* if we supply electromagnetic energy (photons), and simply *field emission* if energy is supplied by an electric field.

[‡]For copper and gold the work function is on the order of 4.5–5.0 eV, and for copper, $E_F \simeq 7$ eV at room temperature.

function $e\phi$. The shading below E_F in the metal indicates that energy levels below E_F are filled with electrons, since E_F is the energy of the most energetic electrons.

Therefore, for example, thermal emission involves supplying sufficient thermal energy such that the electron's energy is raised at least $e\phi$ above the level E_F, and then the electron can escape from the metal. Thus, in this case, the electron effectively goes *over the barrier*, and the electron emerges from the metal with energy greater than or equal to $E_F + e\phi$ (depending on how much energy is supplied).

If an insulator replaces the vacuum, then the work function is replaced with a *reduced (or modified) work function* $e\phi'$, which is the energy required to liberate an electron from the metal's surface into the insulating region (i.e., into the conduction bandedge of the insulator (Section 5.4)). For example, since the electron affinity, $e\chi$, of SiO_2 is 0.9 eV, the modified work function of a metal–SiO_2 junction is $e\phi' = e\phi - e\chi = e\phi - 0.9$. The modified work function for several metal–SiO_2 junctions is shown in Table 6.2.

Furthermore, if the vacuum region is replaced by a semiconductor, the resulting metal–semiconductor junction behaves in a similar manner to the metal–insulator junction, although the energy bands on the semiconductor side become curved, rather than forming straight lines, and the barrier height is approximately one-half of the bandgap energy. For example, Fig. 6.5 shows the energy band diagram for a metal–semiconductor junction before the materials are joined (the semiconductor is assumed to be n-type, and $e\phi_m > e\phi_s$), and Fig. 6.6 shows the junction after the two materials are brought together and thermal equilibrium is established.

The band bending on the semiconductor side is due to the fact that upon contact, charges will flow across the junction (in this case, electrons from the semiconductor will cross into the metal, since $E_c > E_{F,\,\text{metal}}$) until the Fermi levels of the two materials are aligned. For this example, electrons are depleted from the semiconductor near to the interface, resulting in a net positive charge and an upward bending of the energy bands near to, and on the semiconductor side of, the interface. There is no band bending on the metal side, since, for instance, there is no voltage drop in the metal.[†] This results in a barrier (called a

TABLE 6.2 WORK FUNCTION FOR A METAL-VACUUM INTERFACE, AND MODIFIED (REDUCED) WORK FUNCTION FOR A METAL-SiO_2 INTERFACE (FROM [9]).

Metal	$e\phi$ (eV)	$e\phi'$ (eV)
Al	4.1	3.2
Ag	5.1	4.2
Au	5.0	4.1
Cu	4.7	3.8

Goser, K., P. Glösekötter, and J. Dienstuhi (2004). *Nanoelectronics and Nanosystems—From Transistors to Molecular and Quantum Devices*, Berlin: Springer-Verlag.

[†]If the metal is approximated as a perfect conductor, there is no band bending on the metal side. However, if the metal is more accurately modeled as an imperfect conductor, band banding does occur, but is limited to a very small region near the surface of the metal.

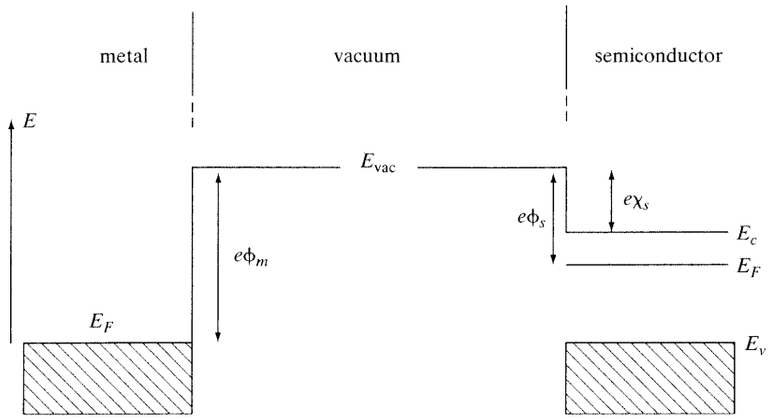

Figure 6.5 Metal–semiconductor junction before contact.

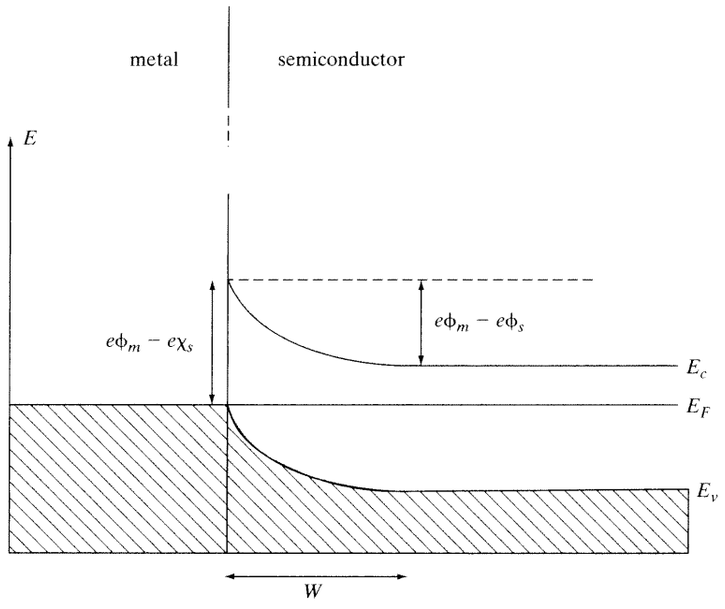

Figure 6.6 Metal–semiconductor junction after contact at thermal equilibrium.

Schottky barrier) to electron flow, with the barrier height given by

$$e\phi_b = e\phi_m - e\chi_s. \tag{6.28}$$

The depleted region is called a *space charge layer*, and has approximate width W. The exact form of the energy band profile in the depletion region must be obtained by solving Poisson's equation for the charge profile, and will not be discussed here.† The resulting junction is called a *Schottky diode*, since upon applying a voltage bias positive with respect to the metal, the barrier will be lowered,‡ allowing large currents to flow metal to semiconductor (i.e., for electrons to cross from the semiconductor to the metal), and applying a voltage bias negative with respect to the metal, the barrier will be raised, impeding current flow.

Many applications require an *ohmic contact*, in which current can flow in either direction with very little resistance. Being able to align the energy levels of the metal and semiconductor would help accomplish this, but interface effects also play a role. Often ohmic contacts are made by heavily doping the semiconductor near the metallic contact.

In summary, the junction between two materials presents a change in potential energy, and results in either a step change in energy, as in the case of a metal–vacuum or metal–insulator junction, or a more complicated energy profile, such as for a metal–semiconductor junction. It can then be seen that the energy profile depicted in Fig. 6.2 on page 185 is a model for a metal–vacuum–metal junction, as shown in Fig. 6.7 (assuming identical metals in thermal equilibrium on either side of the vacuum region).

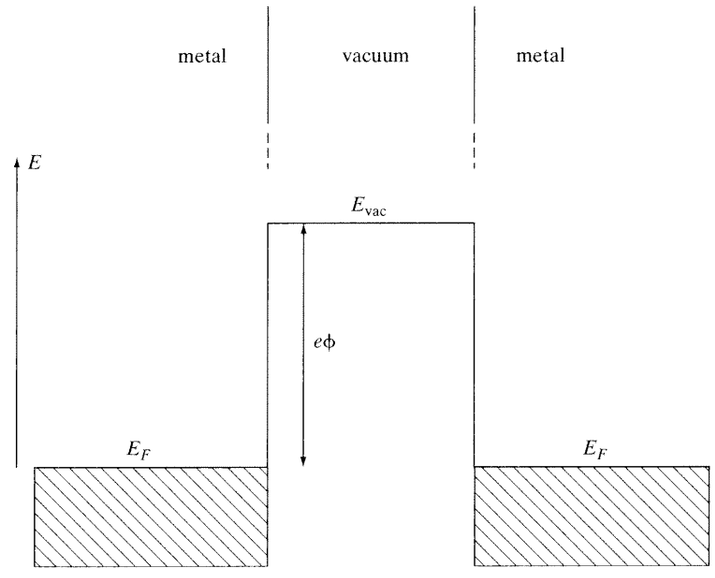

Figure 6.7 Metal–vacuum–metal junction.

†This is standard material in semiconductor device physics texts.
‡See Section 5.4.3 for the effect of an applied voltage on energy bands.

A metal–insulator–metal structure would have a very similar energy profile, although the modified work function of the metals, $e\phi'$, would replace the work function $e\phi$. A metal–semiconductor–metal junction would also lead to a similar profile, although with band bending in the semiconductor.

To consider the effect of an applied field on a material junction, we can examine the metal–vacuum–metal junction in Fig. 6.7. In this case, it is convenient to consider applying a voltage V_0 across the vacuum region, resulting in the electric field magnitude $\mathcal{E}_0 = V_0/d$, where d is the thickness of the vacuum region. Combining this result with the work function then leads to the total potential energy profile

$$e\phi - q_e V_0 x/d \tag{6.29}$$

in the vacuum region. Of course, a similar result holds if the vacuum is replaced by an insulating material, with the resulting band diagram shown in Fig. 6.8. If the insulator were a vacuum, then the barrier height would extend up to the vacuum level, i.e., $e\phi' = e\phi$.

At this point, it is worthwhile to consider the possible tunneling currents that arise in a metal–insulator–metal junction under an applied bias. Three possible currents (I_1, I_2, and I_3) are shown in Fig. 6.8. We assume that in each metal region, all states below E_F are filled and all states above E_F are empty. As such, we must have $I_1 = 0$, since this current would result from the flow of electrons having energy above E_F; however, these energy states are empty. Current I_3 would result from filled states on the left tunneling into already filled states on the right, and so, since this is impossible, $I_3 = 0$ as well. The actual

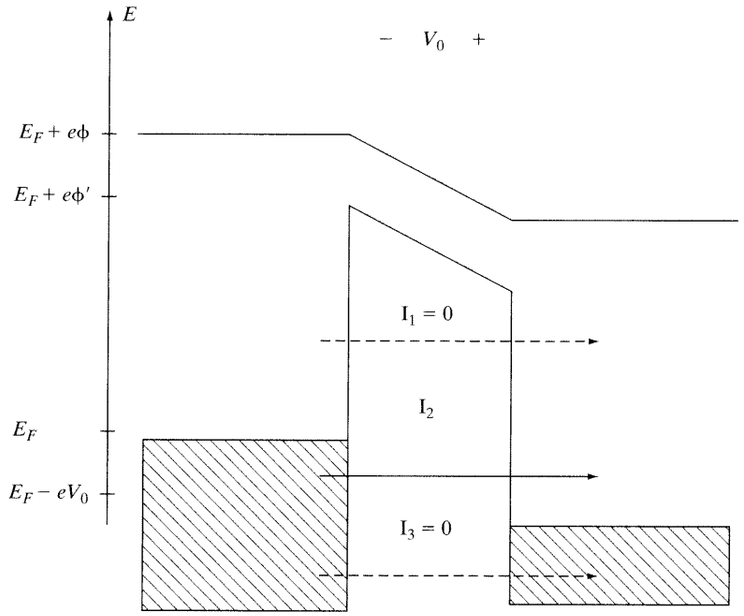

Figure 6.8 Metal–insulator–metal junction band diagram for an applied voltage V_0. Bias is positive on right side, and negative on left side.

tunneling current arises from *filled* states on the left tunneling into *unfilled* states on the right, resulting in tunneling current I_3.

6.3 APPLICATIONS OF TUNNELING

As described briefly earlier, there are many applications of tunneling, especially in the emerging area of nanoelectronics. Tunneling can be used for beneficial purposes, or it can be detrimental to device performance. Next we briefly examine several different aspects of tunneling.

6.3.1 Field Emission

Excepting Fig. 6.8, the energy profiles described in the previous section correspond to the case of no applied field or bias. That is, the energy profile reflects the junction after the materials are joined together, and after thermal equilibrium is established, which equalizes the Fermi levels. However, as might be guessed from Section 5.4.3, the presence of an electric field or voltage modifies the band structure. In particular, we know that an electric field or voltage tilts energy bands, depressing the energy band on the positive side of the field. Therefore, if an electric field or voltage is applied across the junction between a metal and a vacuum, due to (6.29), the potential energy profile becomes triangular, as shown in Fig. 6.9.

As described previously, if energy $E_F + e\phi$ or more is supplied to the structure, an electron can *go over* the energy barrier, as depicted in Fig. 6.10. However, note that as the applied electric field magnitude is increased, the slope of the energy profile in Fig. 6.9 becomes greater, and the triangular barrier becomes thinner. Thus, for a sufficiently large electric field, electrons can easily tunnel *through* the thin barrier, as depicted in Fig. 6.11. This is called field emission, or *cold emission*, since the electrons emerge from the metal with energies lower than $E_F + e\phi$. This is also called *Fowler–Nordheim* (FN) *tunneling*, named after the researchers who investigated field emission in the 1920s. It can be shown that the tunneling probability through the triangular barrier depicted in Fig. 6.9 is[†]

$$T = \exp\left(\frac{-4\sqrt{2m_e^*}}{3\,|q_e|\,\mathcal{E}\hbar}\,(e\phi - (E - E_F))^{3/2}\right), \tag{6.32}$$

[†]This result comes from the Wentzel–Kramers–Brillouin (WKB) approximation of the wavefunction $\psi(x)$ in a region of slowly varying potential energy $V(x)$. This is described in standard textbooks on quantum mechanics, and the main result is that for a tunnel barrier extending from x_1 to x_2,

$$T \simeq e^{-2\int_{x_1}^{x_2}\beta(x)dx}, \tag{6.30}$$

where

$$\beta(x) = \sqrt{\frac{2m^*}{\hbar^2}\,(V(x) - E)}. \tag{6.31}$$

When $V(x)$ has a triangular shape, (6.32) results. Although the discontinuity in V violates the condition of $V(x)$ being slowly varying, the result is approximately correct.

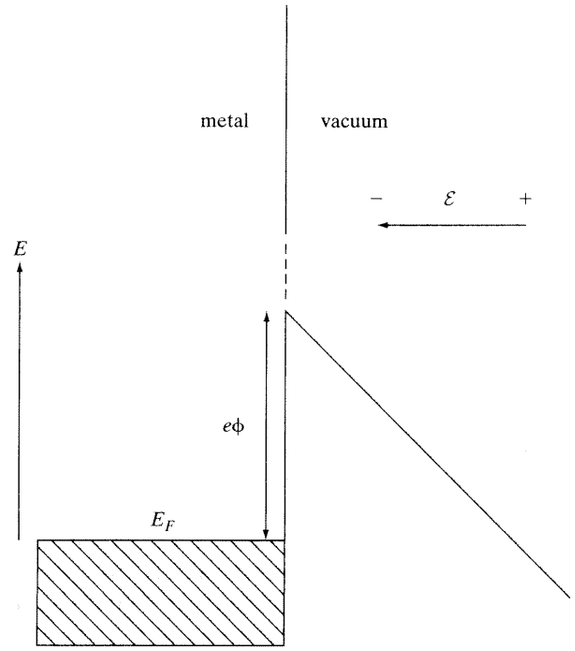

Figure 6.9 Metal–vacuum interface in the presence of an applied electric field $\mathcal{E}$.

where E is the energy of the electron (often the case $E = E_F$ is of interest), $e\phi$ is the barrier height, and $\mathcal{E}$ is the magnitude of the electric field. If the vacuum region is replaced by an insulator, then we use the metal–insulator work function $e\phi'$, rather than $e\phi$.

A good application of Fowler–Nordheim tunneling is to the description of field emission by carbon nanotubes. As described in Section 5.5, carbon nanotubes have nanoscopic radius values, and thus possess an extremely sharp tip that concentrates the electric field to a very small region of space. This strong field enhances tunneling through the vacuum barrier. As an example, an SEM image of the apparatus to measure the field emission I–V characteristics of an individual carbon nanotubes is shown in Fig. 6.12, along with the best fit Fowler–Nordheim result. The field-emitted current begins at approximately 91 V, and saturates around 150 V.

To apply the Fowler–Nordheim result to model this situation, we must obtain the tunneling current. In general, tunneling current is related to the product of the incident electron density multiplied by the tunneling probability, which is then integrated over various states.[†] For the triangular-like barrier presented by field emission, the result is[‡]

$$I = A\frac{1.5 \times 10^{-6}}{e\phi}\mathcal{E}^2 \exp\left(\frac{10.4}{\sqrt{e\phi}}\right)\exp\left(-6.44 \times 10^9 \frac{(e\phi)^{3/2}}{\mathcal{E}}\right), \tag{6.33}$$

[†]The method for determining tunneling current is the same as that described in Section 10.2.3 for a slightly different application; the basic equation for tunneling current is (10.49), where the limits of integration may change to account for the bandstructure of the material.

[‡]See [11]–[14].

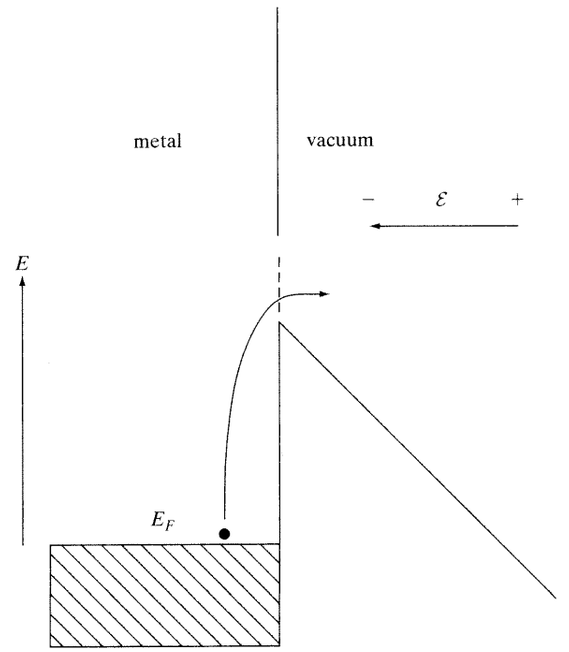

Figure 6.10 Metal–vacuum interface in the presence of an applied electric field $\mathcal{E}$, where an electron at the Fermi level goes over the potential barrier.

where A has the dimension of area (m^2) and the work function $e\phi$ has units of electron volts. The local field $\mathcal{E}$ is related to the applied field V/d by $\mathcal{E} = \gamma V/d$, where the *field enhancement factor* γ quantifies the ability of the emitter to intensify the applied field. For the results shown in Fig. 6.12, $e\phi = 4.9$ eV, $\gamma = 90$, and $A = 5 \times 10^{-16}$ m^2. These values are obtained from the measurement by noting that

$$\ln\frac{I}{V^2} = \ln\left(A\frac{1.5 \times 10^{-6}}{e\phi d^2}\gamma^2\right) + \left(-6.44 \times 10^9 \frac{(e\phi)^{3/2} d}{\gamma}\frac{1}{V} + \frac{10.4}{\sqrt{e\phi}}\right), \tag{6.34}$$

or

$$\ln\frac{I}{V^2} = c_1 + \left(-c_2\frac{1}{V} + c_3\right), \tag{6.35}$$

where c_1–c_3 are constants. Thus, a plot of $\ln(I/V^2)$ versus $1/V$ should be linear with a negative slope. In the insert of Fig. 6.12, the experimental $\ln(I/V^2) - (1/V)$ curve is shown, which indeed has the desired behavior. Since d is known for the measurement system, and the approximate value of the work function for the CN is known, γ can be determined from

$$c_2 = 6.44 \times 10^9 \frac{(e\phi)^{3/2} d}{\gamma}, \tag{6.36}$$

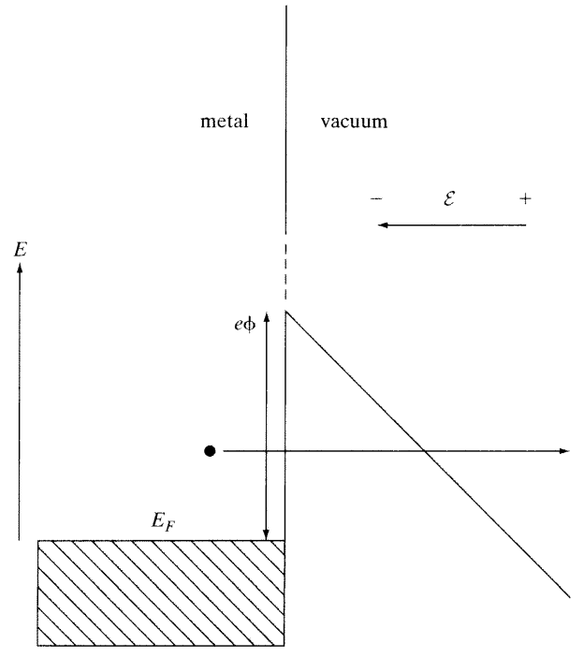

Figure 6.11 Metal–vacuum interface in the presence of an applied electric field $\mathcal{E}$, where an electron at the Fermi level tunnels through the potential barrier.

where c_2 is obtained from the measured slope. Then, A is determined from the constant

$$c_1 = \ln\left(A\frac{1.5\times10^{-6}}{e\phi d^2}\gamma^2\right), \tag{6.37}$$

since the constant $c_3 = 10.4/\sqrt{e\phi}$ is known.

The issue of emission stability and device lifetime is a possible concern for CN field emitters. While continuous operation without degradation of CN field emission sources has been demonstrated for time frames exceeding one year, single emitters and CN arrays have been observed to fail for reasons that are not currently well understood. Failure may be due to CN tip damage by large emission currents, although the tube environment (gas concentration, temperature, etc.) seems also to play a role. Nevertheless, it is expected that tunneling-based carbon nanotube flat-panel displays may be commercially available in the near future. Other devices, such as flash memories that use tunneling, have been commercially available for some time.

6.3.2 Gate–Oxide Tunneling and Hot Electron Effects in MOSFETs

Tunneling is a very important aspect in MOSFETs and similar structures, especially as the feature size is reduced. Consider the usual n-type MOSFET structure shown in Fig. 6.13, where s, d, and g indicate the source, drain, and gate, respectively.

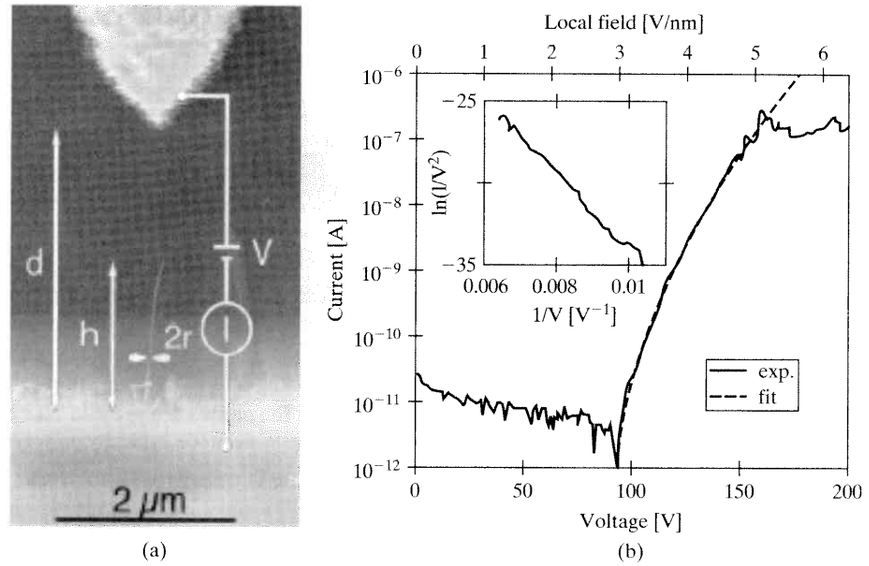

Figure 6.12 (a) SEM image of the experimental setup for measuring field-emission I–V characteristics of an individual carbon nanotube. The nanotube length is $h = 1.4$ μm, and the tube radius is 7.5 nm, with the anode positioned at $d = 2.65$ nm. (b) Experimental I–V characteristics (solid line) and the best fit Fowler–Nordheim prediction (dashed line; $e\phi = 4.9$ eV, $\gamma = 90$, and $A = 5\times10^{-16}$ m^2) for an individual MWNT. The insert of (b) is described in the text. (From Bonard, J. M. et al., "Field Emission of Individual Carbon Nanotubes in the Scanning Electron Microscope," *Phys. Rev. Lett.* 89 (2002): 197602. Copyright 2002, American Physical Society.)

The oxide layer is conventionally formed by oxidizing the silicon substrate, forming an SiO_2 insulating barrier between the gate electrode and the rest of the device.[†] As shown in Fig. 6.13, there is no conduction channel between the source and the drain (both n-type Si) when the gate voltage V_g is zero; thus, $I_{ds} = 0$ irrespective of V_{ds}. When a positive gate voltage $V_g > 0$ is applied, and has sufficient magnitude,[‡] an inversion layer is formed under the gate, connecting the source and drain. The inversion layer is formed since positive voltage V_g pushes away holes, and attracts electrons under the gate, forming, in effect, an n-type channel, as shown in Fig. 6.14. This allows current flow in the induced channel from drain to source upon applying a potential $V_{ds} > 0$. From an energy barrier viewpoint, when $V_g = 0$, there is a large energy barrier between source and drain. As V_g is increased, this barrier is pushed down, eventually below the filled states of the source and drain, and conduction can take place. MOSFET characteristics are reviewed in Appendix C.

Considering the gate–oxide–channel junction, we have something like a metal–insulator–metal junction, and, therefore, the potential energy profile of Figures 6.7 and

[†]High dielectric constant insulators are being developed for MOS devices that will likely replace SiO_2, allowing for thicker oxide layers resulting in less tunneling.

[‡]In order to induce a channel, we need $V_g > V_t$, where V_t is called the *threshold voltage*, where typically V_t is on the order of a volt.

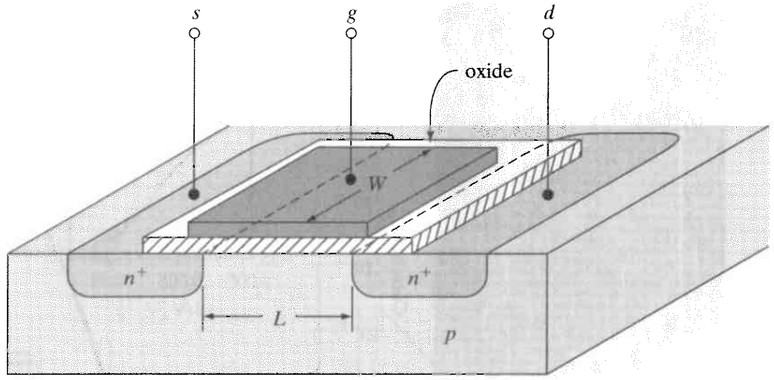

Figure 6.13 Physical structure of an n-type MOSFET. The regions denoted as n^+ are heavily doped, n-type Si, and p denotes the p-type Si substrate. For the gate electrode, typically polycrystalline silicon (polysilicon) is used for a variety of technical reasons.

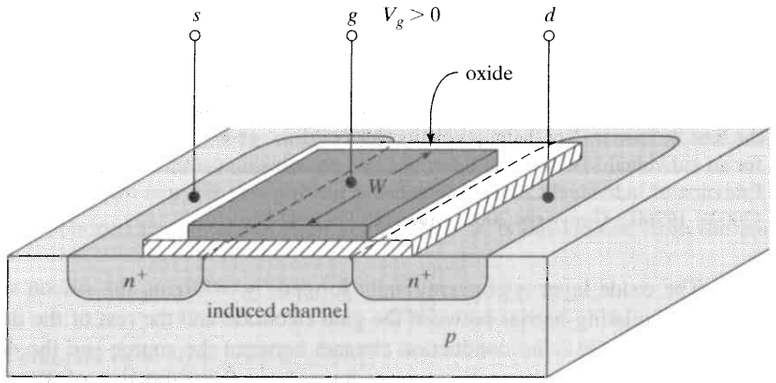

Figure 6.14 MOSFET with positive gate voltage, creating a n-type conducting channel between source and drain.

6.8 approximately applies. That is, for simplicity, we are modeling the inverted p-type semiconductor channel as a metal. A more careful analysis would take into consideration the fact that the channel is actually a semiconductor, and the band diagram would differ a bit on the channel side due to band bending.

Of course, in an ideal classical MOSFET, electrons do not travel between the channel and the gate (i.e., $I_g = 0$) because of the presence of the insulating oxide region. However, in light of our previous discussions, it is obvious that for sufficiently thin oxides, electrons will be able to cross (tunnel through) this energy barrier, leading to[†] $I_g \neq 0$. There are several

[†]This tunneling current is in addition to any current that may be present due to the oxide being an imperfect insulator, perhaps due to the presence of trapped charge impurities and other defects.

possible effects relating to quantum tunneling through the oxide, and next we mention two of these.

Hot Electrons. Drain-source current obviously results from accelerating electrons via the source-drain voltage, V_{ds}, which results in a horizontal electric field in the channel. As these electrons are accelerated, they gain kinetic energy. If they gain sufficient kinetic energy, they may tunnel through the oxide.[†] They may gain a large amount of kinetic energy from either a large V_{ds} and correspondingly large horizontal electric field ($\mathcal{E}_{ds} \propto V_{ds}/L$, where L is the channel length), or from a short channel. Note that this effect is also influenced by the presence of the vertical electric field in the oxide due to V_g. The end result is that electrons that are supposed to transverse the channel and reach the drain may, because of their high kinetic energy, instead tunnel through the oxide and contribute to an undesired gate current, as shown in Fig. 6.15. This is called the *hot-electron effect*, since the highly energetic electrons are considered "hot."

Fowler–Nordheim Tunneling. The second possibility is that, if a strong gate voltage is applied, electrons will be energetic enough from this field alone to become likely to tunnel through the oxide, as depicted in Fig. 6.16.

It is obvious that nonzero gate current can be attributed to a combination of tunneling events (as well as defects, trapped charge states, etc.), all of which lead to significant gate currents if the oxide layer is sufficiently thin. An accurate analysis results from a self-consistent numerical solution of coupled Poisson and Schrödinger's equations. Poisson's equation is used to obtain the potential profile, and an effective mass Schrödinger's equation provides the wavefunction, from which the probability current can be obtained using (3.187). In some cases a Fowler–Nordheim model provides reasonable accuracy. (One major cause

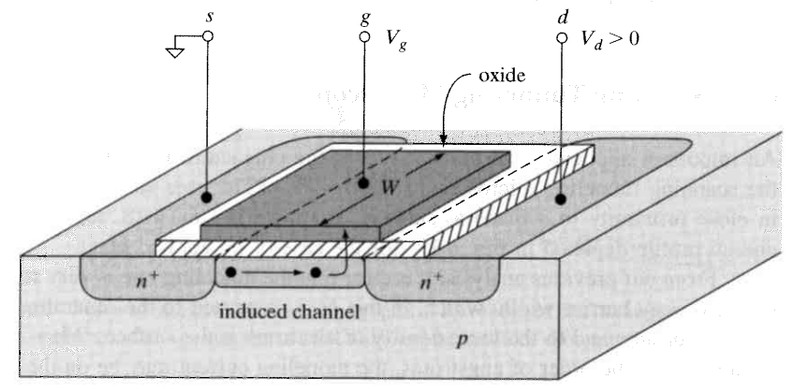

Figure 6.15 Depiction of the hot-electron effect, where electrons transversing the channel gain sufficient energy from the source-drain electric field to tunnel through the oxide energy barrier.

[†]Recall that tunneling is a random process, and that, for any energy, the electrons may tunnel. However, the tunneling probability goes up if the electrons' energy increases, or if the barrier thickness decreases.

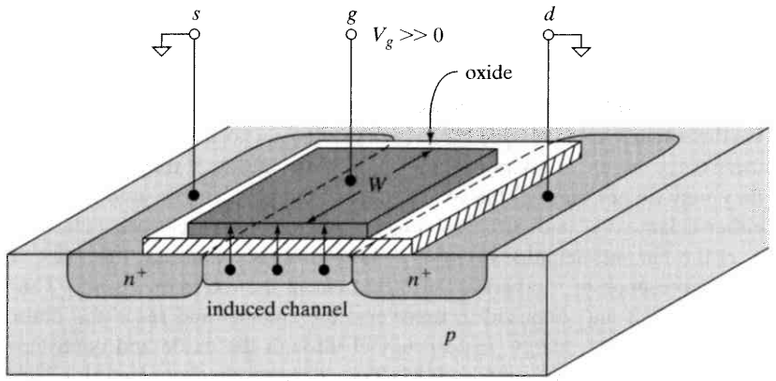

Figure 6.16 Depiction of Fowler–Nordheim tunneling. Strong gate voltage provides electrons in channel with sufficient energy to tunnel across the oxide energy barrier.

of inaccuracy in the Fowler–Nordheim model is that the potential energy profile is assumed, rather then obtained rigorously.)

For typical oxides, thickness values less than approximately 1.5 nm lead to relatively high tunneling rates. However, tunneling can occur even for moderately thick oxides if the gate voltage is high. For example, Fig. 6.17 shows gate current versus gate voltage for an n^+-poly silicon gate (doping concentration is 1×10^{21} cm^{-3}) n-type MOSFET structure, with oxide thickness values of 5, 8, and 10 nm. It can be seen that the Fowler–Nordheim tunneling model[†] (symbols) agrees well with the measured values (solid curves).

Gate current severely impacts standby power consumption and device functionality. The semiconductor industry is considering a variety of approaches to combat this problem, including using new oxide materials, and different MOSFET structures.

6.3.3 Scanning Tunneling Microscope

An important application of tunneling is to the characterization of material surfaces using the scanning tunneling microscope (STM).[‡] The STM uses an extremely fine metallic tip in close proximity to a material surface, as shown in Fig. 6.18, resulting in the potential energy profile depicted in Fig. 6.19 (for the case of no applied bias).

From our previous analysis, it is clear that the tunneling rate is very strongly dependent on the energy barrier width, which, in this case, is related to the separation between the tip and the surface, and to the local density of electrons at the surface. When the tip-to-surface distance is on the order of angstroms, the tunneling current may be on the order of nA, and

[†]This particular Fowler–Nordheim model is actually somewhat of a hybrid model, and is based on parameters obtained from the self-consistent numerical solution of the coupled Poisson and Schrödinger's equations (assuming $m_e^* \simeq 0.5m_e$ for the electron effective mass in the $Si0_2$ oxide).

[‡]In 1986, the Nobel prize in physics was awarded to Gert Binnig and Heinrich Röher at IBM Zürich for their work on developing the STM.

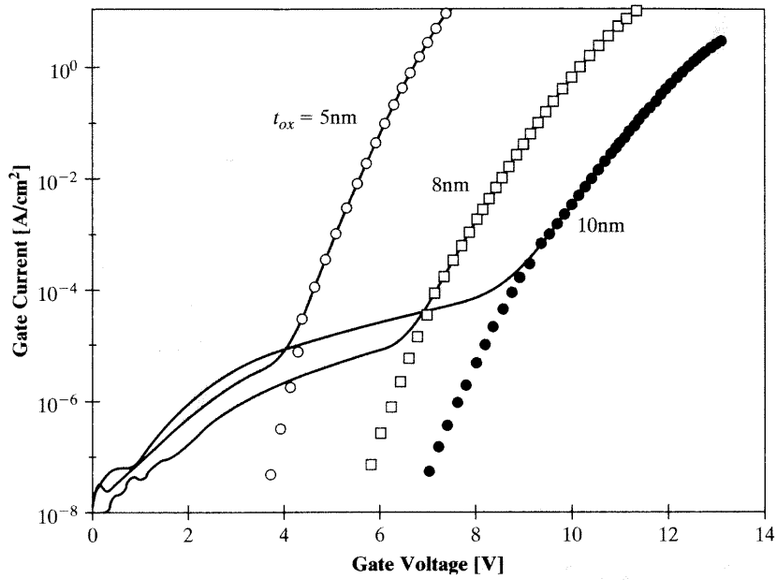

Figure 6.17 Gate tunneling current versus gate voltage for an n^+-poly silicon gate (doping concentration is 1×10^{21} cm^{-3}) n-type MOSFET with oxide thickness values of 5, 8, and 10 nm. The silicon substrate is doped at concentrations of 5×10^{17} cm^{-3}, 3.5×10^{17} cm^{-3}, and 1×10^{-17} cm^{-3}, respectively. The solid curves are measured values, and the symbols are from a Fowler–Nordheim tunneling model. (From Quan, W.-Y., D. M. Kim, and M. K. Cho, "Unified Compact Theory of Tunneling Gate Current in Metal–Oxide-Semiconductor Structures: Quantum and Image Force Barrier Lowering," *J. Appl. Phys.* 92 (2002): 3724. Copyright 2002, American Institute of Physics.)

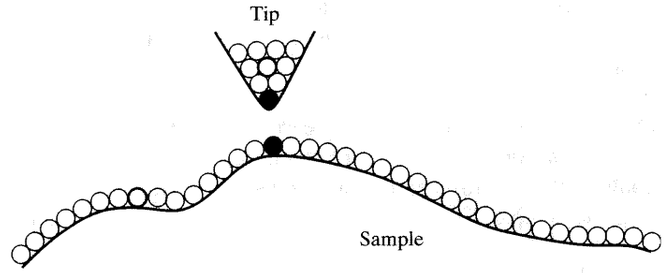

Figure 6.18 Material sample interrogated by probe tip. Most of the tunneling arises between the bottommost atom in the tip, and the nearest atom on the surface, shown in black.

will be very sensitive to the tip-to-surface separation. Thus, as long as the tip position can be controlled to angstrom precision, the surface can be mapped in atomic detail.

It can be appreciated that the STM can function either by moving the tip at a constant height and measuring the change in tunneling current as the tip-to-surface separation varies due to surface features, or by attempting (via feedback) to keep the current constant by

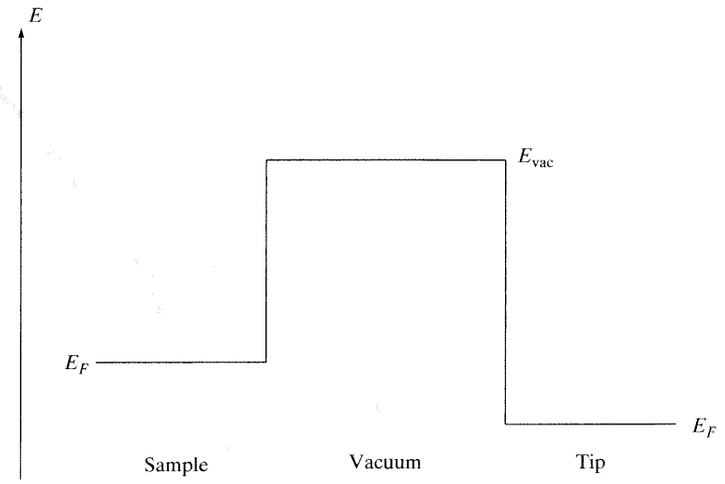

Figure 6.19 Energy diagram for a scanning tunneling microscope. Tunneling occurs between the sample and the tip, surmounting the work function of the material–vacuum interface. Diagram shown for the case of no applied bias.

varying the tip height. In the first method, as the tip moves from location to location on the surface, the amount of tunneling current will become bigger or smaller depending on the local electron density, which is itself related to the positions of the atoms. For example, since the tunneling current falls off exponentially with distance, when the tip is over an atom, the current will be much larger than when the tip is between atoms. However, because of the exponential dependence of the tunneling current, this results in an image in which the atomic peaks look much higher than their actual height. (A true image would result if the tunneling current depended linearly, rather than exponentially, on the sample–tip separation.)

In the constant current method, a piezoelectric crystal is used to vary the tip height, in order to maintain a constant tunneling current. The piezo electric material expands linearly as a function of applied voltage, and, therefore, the voltage needed to expand the crystal (thus moving the tip) to keep the current constant varies linearly with the position of the atoms on the sample. This voltage can be used to record the height of the tip, which is related to the surface features.

Note that the STM image is really an image of the local electron density, and not explicitly a tomographic map of the surface. Therefore, it can be used to image the local density of states, as described further in Section 8.1. For example, if an oxygen atom is located on a metal surface, it will appear as a depression in an STM image, even though the atom is on top of the metal surface. This is because the tip needs to move closer to the surface to maintain the same tunneling current, due to the (roughly) insulting properties of the oxygen atom. Therefore, although the STM itself does not need a vacuum to operate, the STM is often operated in an ultrahigh vacuum to avoid contamination of the sample from the surrounding environment.

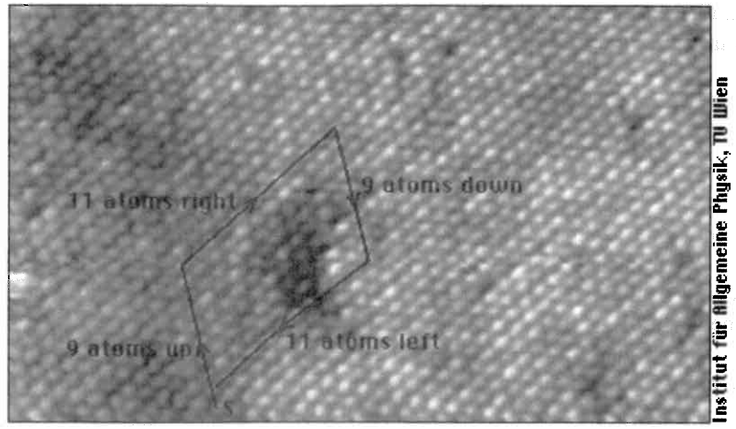

Figure 6.20 STM image of a dislocation in a PtNi alloy. (Courtesy Institut für Allgemeine Physik, Vienna University of Technology.)

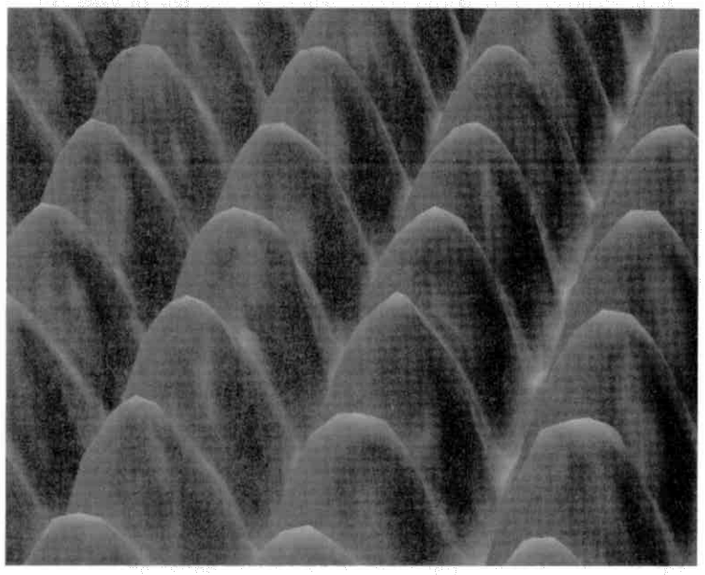

Figure 6.21 STM image of a nickel surface. (Image reproduced by permission of IBM Research, Almaden Research Center. Unauthorized use not permitted.)

Figure 6.20 shows an STM image of a dislocation in a PtNi alloy, and Fig. 6.21 shows an STM image of the surface of nickel.

Similar in application, although not in operating principles, is the atomic force microscope (AFM). In AFM, a cantilever with a sharp tip is brought into close proximity to a sample surface. The force between the tip and the sample leads to a deflection of the

cantilever according to Hooke's law. The deflection may be measured, for example, using a laser.

6.3.4 Double Barrier Tunneling and the Resonant Tunneling Diode

An interesting case occurs when one considers two barriers separated by a small distance, forming a potential well as shown in Fig. 6.22. This leads to the topic of *resonant tunneling*.

We assume that the barriers are sufficiently thin to allow tunneling, and that the well region between the two barriers is also sufficiently narrow to form discrete (quasi-bound) energy levels, as shown in Fig. 6.23.

The analysis of the double barrier structure shown in Fig. 6.22 is essentially the same as considered at the beginning of Section 6.1, although we now have five regions

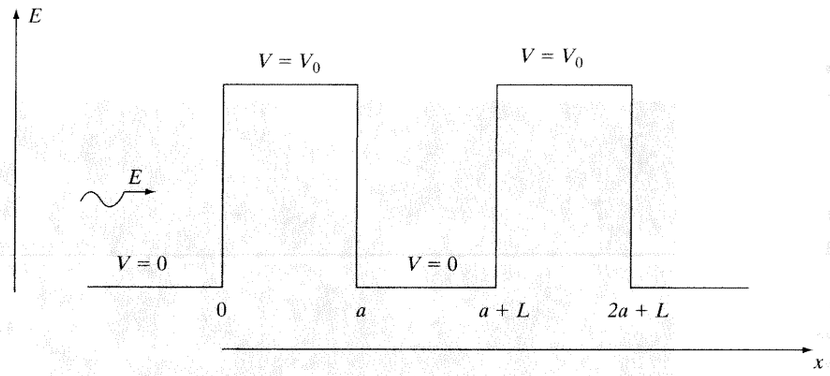

Figure 6.22 Double barrier system forming a potential well.

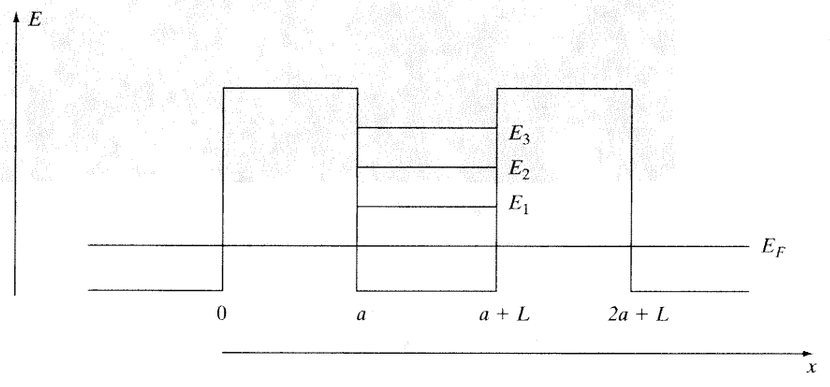

Figure 6.23 Double barrier structure forming a sufficiently narrow well so that energy levels in the well are well quantized. Energy levels E_1, E_2, and E_3 depict quasi-bound states.

to consider, with four interfaces at which to match boundary conditions. Therefore, the analysis is straightforward but tedious. The result for the transmission coefficient of the double symmetric barrier shown in Fig. 6.22 is

$$T = \left(1 + \frac{4R_1}{T_1^2}\sin^2(k_1 L - \theta)\right)^{-1}, \tag{6.38}$$

where T_1 and R_1 are the transmission and reflection coefficients for a single barrier of width a, given by (6.15) and (6.16), respectively; L is the length of the well between the barriers, and

$$\tan\theta = \frac{2k_1k_2\cos(k_2a)}{(k_1^2 + k_2^2)\sin(k_2a)}, \tag{6.39}$$

where

$$k_1^2 = \frac{2m_e^* E}{\hbar^2}, \quad k_2^2 = \frac{2m_e^*(E - V_0)}{\hbar^2}. \tag{6.40}$$

From (6.38), it is easy to see that the transmission probability becomes unity when

$$\sin(k_1 L - \theta) = 0, \tag{6.41}$$

that is, when

$$k_1 L - \theta = n\pi, \quad n = 0, 1, 2, \ldots . \tag{6.42}$$

It turns out these transmission peaks ($T = 1$) will occur when the energy of the incoming electron wave (E) coincides with the energy of one of the quasi-bound states formed by the well. To see this for a simple special case, assume that $V_0 \gg E$, such that $|k_2| \gg |k_1|$. Then, $\tan\theta \to 0$ such that $\theta \to 0$, leading to

$$k_1 L = n\pi.$$

Using the expression for k_1, we see that

$$E = E_n = \frac{\hbar^2}{2m_e^*}\left(\frac{n\pi}{L}\right)^2, \tag{6.43}$$

which is exactly the same as the result for the quantized energy levels in a one-dimensional quantum well (4.35).

The double barrier tunnel junction has important applications to a device known as a *resonant tunneling diode*. The operation of these diodes can be appreciated from considering the influence of bias on the energy band diagrams for the double barrier system. We make use of the fact that when the incident energy E is very different from the energy of a quasi-bound state E_n, transmission will be low, and as $E \to E_n$, transmission will increase, becoming a maximum when $E = E_n$. For example, assume that incident electrons have energy E, and that, at first, all of the quasi-bound states E_n lie above E, as shown in Fig. 6.24.

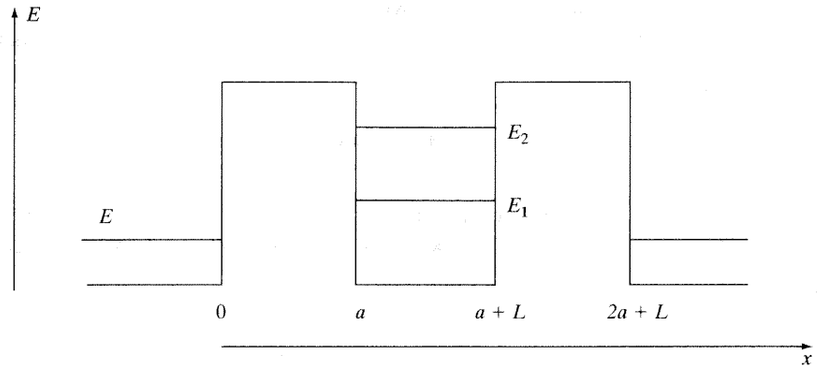

Figure 6.24 Double barrier junction with no applied bias. E is the energy of the incident electron, and $E_{1,2}$ are the energy levels of the quasi-bound states in the well.

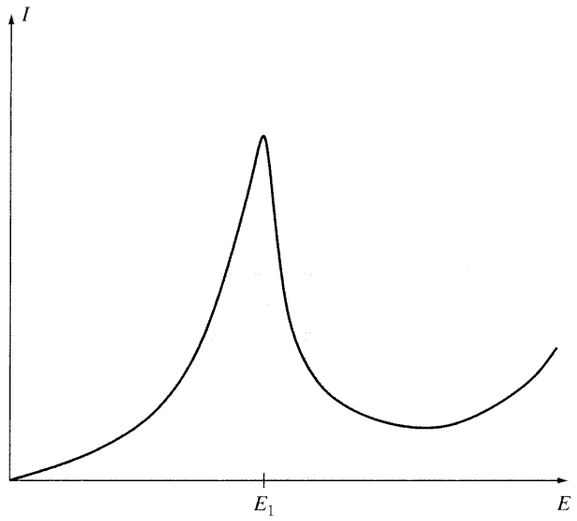

Figure 6.25 Current–energy characteristic for a resonant tunneling junction, where E is the energy of the incident electron and E_1 is the energy level of the first quasi-bound state in the well.

As E increases, tunneling will increase, reaching a peak when $E = E_1$. After that point, a further increase in E will result in a decreasing current, as shown in Fig. 6.25. This decrease of current with an increase of bias is called *negative resistance*. Further peaks and valleys will occur as $[E]$ approaches, and then moves past, other quasi-bound states.

A typical structure is made by using n-type GaAs for the regions to the left and right of both barriers, intrinsic GaAs for the well region, and AlGaAs or AlAs for the barrier material. Tunneling is controlled by applying a bias voltage across the device. For the case of no applied bias, the energy band diagram is similar to that shown in Fig. 6.24.

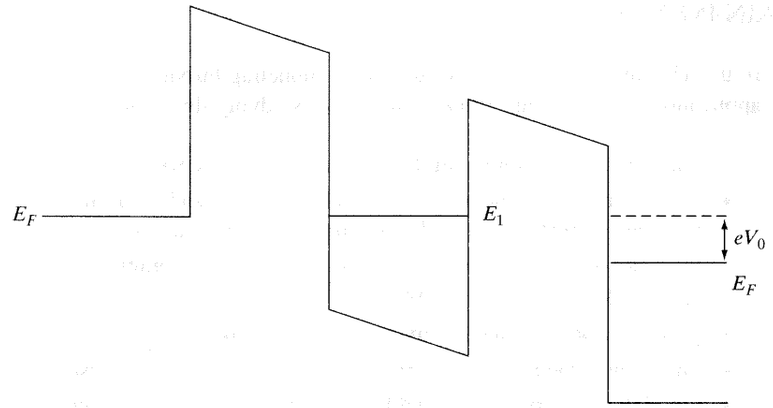

Figure 6.26 Double barrier junction under the action of an applied bias.

For an applied bias V_0, positive on the right side of the double junction, an appreciable current begins to flow when the quasi-bound state is pulled down to the Fermi level of the left region, as shown in Fig. 6.26. Current reaches a maximum when the level of the quasi-bound state is equal to the conduction bandedge of the left region.

Superlattice. Going beyond a double barrier structure is a periodic array of barriers, forming what is known as a *superlattice*. If enough layers are used, this structure results in periodic behavior (and associated band formation), as was found for crystalline materials in Chapter 5. The result is a one-dimensional artificial crystal, although the period is much longer than that found for a crystal (whose periodicity is governed by interatomic spacing).

As a simple approximate analysis, the Kronig–Penney model (Fig. 5.7 on page 138) can be used, where the barrier thickness a_2 and the well thickness a_1 correspond to the thickness of the material layers. Typically, a large bandgap and a small band gap material is used (i.e., alternating layers of a large bandgap material having thickness a_2, and a small bandgap material having thickness a_1). The analysis presented in Section 5.3 is appropriate for an infinite superlattice, or for a sufficiently long structure. The analysis of a finite superlattice can be done using the method described in Section 6.1, although efficient matrix methods can be used to avoid generating large numbers of simultaneous equations.

As a rough approximation, we can consider the energy levels formed by one isolated well. Then, using the ideas of the interacting systems model presented in Section 5.4.2, we see that for a collection of N interacting wells, the energy levels split into N discrete levels, and, as N becomes large, energy bands are developed. In this way, an artificial material can be made with specific band characteristics. Bloch oscillations can be sustained in superlattices, since the band structure can be precisely controlled. (An important aspect is the size of the first Brillouin zone.) Superlattice structures have been used as infrared oscillators and detectors, in various optical and quasi-optical devices, in transistor applications, and in a host of other areas, including heterostructure fabrication and material coatings. Heterostructures are introduced in Chapter 9.

6.4 MAIN POINTS

In this chapter, we have examined particle tunneling through barriers, and implications and applications of tunneling. In particular, after studying this chapter, you should understand

- quantum particle tunneling through simple energy barriers;
- energy profiles as models of material interfaces, and what material junctions are represented by rectangular and triangular energy profiles;
- field emission, and applications to carbon nanotube emitters;
- gate-oxide tunneling in MOSFETs;
- principles of the scanning tunneling microscope;
- tunneling through double barriers, and applications to the resonant tunneling diode;
- the idea of a superlattice, and how it can behave as an artificial crystal.

6.5 PROBLEMS

1. Plot the tunneling probability versus electron energy for an electron impinging on a rectangular potential barrier (Fig. 6.2, page 185) of height 3 eV and width 2 nm. Assume that the energy of the incident electron ranges from 1 eV to 10 eV.

2. Plot the tunneling probability verses barrier width for a 1 eV electron impinging on a rectangular potential barrier (Fig. 6.2, page 185) of height 3 eV. Assume that the barrier width varies from 0 nm to 3 nm.

3. A 6 eV electron tunnels through a 2-nm-wide rectangular potential barrier with a transmission coefficient of 10^{-8}. The potential energy is zero outside of the barrier, and has height V_0 in the barrier. What is the height V_0 of the barrier?

4. Can humans tunnel? Consider running 1 m/s (assume that you have no potential energy) at an energy barrier of 50 J that is 1 m thick.
(a) If you weigh (i.e., your mass is) 50 kg, determine the probability that you will tunnel through the barrier.
(b) Consider that in order for tunneling to have a reasonably large probability of occurring, $k_2 a$ can't be too large in magnitude. Discuss the conditions that would result in this happening.

5. Referring to the development of the tunneling probability through a potential barrier, as shown in Section 6.1, apply the boundary conditions (3.143) to (6.13) to obtain (6.14).

6. Consider the metal–insulator junction shown in Fig. 6.4 on page 190 . Solve Schrödinger's equation in each region (metal and insulator), and derive tunneling and reflection probabilities analogous to (6.15)–(6.16) for this structure.

7. Consider a metal–insulator–metal junction, as shown in Fig. 6.7 on page 193, except assume two different Fermi levels.
(a) Draw the expected band diagram upon first bringing the metals into close proximity.

(b) Because of the difference in Fermi levels, tunneling will occur (assuming that the barrier between the metals is thin), and will continue until a sufficient voltage is built up across the junction, equalizing the Fermi levels. This internal voltage is called the *built-in voltage*. Draw the energy band diagram showing the built-in voltage in this case.

8. Draw the potential energy profile for a metal–vacuum–metal structure when a voltage V_0 is applied across the vacuum region.

9. Determine the tunneling probability for an Al-SiO_2-Al system, if the SiO_2 width is 1 nm and the electron energy is 3.5 eV. Repeat for an SiO_2 width of 2 nm, 5 nm, and 10 nm.

10. Use the WKB tunneling approximation (6.30) to determine the tunneling probability for the rectangular barrier depicted in Fig. 6.2 on page 185.

11. Plot the tunneling probability versus electron energy for an electron impinging on a triangular potential barrier (Fig. 6.9, page 196), where $e\phi = 3$ eV and the electric field is 10^9 V/m. Assume that the energy difference $(E - E_F)$ ranges from 0 to 3 eV.

12. Consider the double barrier structure depicted in Fig. 6.22 on page 206.
(a) Plot the tunneling probability versus electron energy for an electron impinging on the double barrier structure. The height of each barrier is 0.5 eV, each barrier has width $a = 2$ nm, and the well has width 4 nm. Assume that the energy of the incident electron ranges from 0.1 eV to 3 eV, and that the effective mass of the electron is $0.067m_e$ in all regions.
(b) Verify that the first peak of the plot occurs at an energy approximately given by the first discrete bound state energy of the finite-height, infinitely-thick-walled well formed by the two barriers. Use (4.83) adopted to this geometry, i.e.,

$$k_2 \tan(k_2 L/2) = k_1, \tag{6.44}$$

where $L = 4$ nm and

$$k_2 = \sqrt{\frac{2m_e^* E}{\hbar^2}}, \quad k_1 = \sqrt{\frac{2m_e^* (V_0 - E)}{\hbar^2}}. \tag{6.45}$$

13. Derive the tunneling probability (6.38) for the double barrier junction depicted in Fig. 6.22 on page 206.

14. Research how tunneling is used in flash memories, and describe one such commercial flash memory product.

15. Research how field emission is used in displays, and summarize the state of display technology based on field emission.

16. Explain how a negative resistance device can be used to make an oscillator.